Atmos. Meas. Tech., 18, 4907–4922, 2025
https://doi.org/10.5194/amt-18-4907-2025

Atmospheric Measurement Techniques
Open Access

Assimilation of global navigation satellite system (GNSS) zenith delays and tropospheric gradients: a sensitivity study utilizing sparse and dense station networks

Rohith Thundathil[1,2], **Florian Zus**[2], **Galina Dick**[2], **and Jens Wickert**[1,2]

[1]Institute of Geodesy and Geoinformation Sciences, Technische Universität, Berlin,
Kaiserin-Augusta-Allee 104, 10553 Berlin, Germany
[2]Section 1.1 Space Geodetic Techniques, GFZ Helmholtz Centre for Geosciences,
Telegrafenberg, 14473 Potsdam, Germany

Correspondence: Rohith Thundathil (r.thundathil@tu-berlin.de)

Received: 2 January 2025 – Discussion started: 7 February 2025
Revised: 20 May 2025 – Accepted: 8 July 2025 – Published: 30 September 2025

Abstract. The assimilation of global navigation satellite system (GNSS) zenith total delays (ZTDs) into numerical weather models improves weather forecasts. In addition, the GNSS tropospheric gradient (TG) estimates provide valuable insight into the moisture distribution in the lower troposphere. In this study, we utilize a newly developed forward operator for TGs to investigate the sensitivity effects of incorporating TGs into the Weather Research and Forecasting model at varying station network densities. We assimilated ZTD and TGs from dense and sparse station networks (0.5 and 1°, respectively). Through this study, we found that the improvement in the humidity field with the assimilation of ZTD and TGs from the sparse station network (1° resolution) is comparable to the improvement achieved by assimilating ZTD only from the dense station network (0.5° resolution). These results encourage the assimilation of TGs alongside ZTDs in operational weather forecasting agencies, especially in regions with few GNSS stations. Conversely, assimilating TGs alongside ZTDs from sparse GNSS networks can be a cost-effective way to enhance the accuracy of the model fields and subsequent forecast quality.

1 Introduction

Global navigation satellite systems (GNSSs) have become integral to our everyday lives. They significantly revolutionized how we determine our position, navigate, and keep track of time. The most profound application of GNSS has been in civilian and commercial uses, such as positioning, navigation, and timing. However, GNSS is increasingly valuable for geosciences in accurately sensing atmospheric and surface properties and other geophysical parameters. Additionally, it can be used to derive the Earth's surface properties, deformation, and other geophysical parameters (Wickert et al., 2020).

Monitoring atmospheric water vapor with GNSS regional ground networks has helped bridge gaps in established meteorological observing systems. GNSS is distinguished from other observation systems by its numerous benefits, such as low operating costs, all-weather availability, and exceptional spatiotemporal resolution. The total number of GNSS stations worldwide exceeds 10 000. European networks, with about 3000 stations, enhance regional weather forecasts. Incorporating advanced GNSS-based observations allows us to provide high-quality information with a high spatiotemporal distribution in operational weather forecasting models worldwide. This is essential for accurately modeling the atmosphere, especially for predicting heavy precipitation and severe weather events, which are significant challenges in weather research.

Since 1992, GNSS signals have been utilized to monitor the atmosphere through ground-based stations ("GNSS meteorology"). GNSS meteorology uses the time delay of radio signals traveling from the satellite to the station to monitor atmospheric water vapor. Zenith total delay (ZTD) is a key measurement in GNSS meteorology (Bevis et al., 1992), closely linked to the integrated water vapor (IWV) above the station. ZTD data are available in near real-time (NRT) from several European station networks, such as the European Meteorological Network Global Navigation Satellite Systems Water Vapor Program (EGVAP). Once adjusted for ionospheric effects, the delay caused by the troposphere in transmitting GNSS signals between satellites and stations is estimated. The ZTD has been utilized by various operational forecast agencies. Several assimilation studies have been performed with ZTDs and found that they enhance the accuracy of the forecasts. For example, Vedel and Huang (2004) showed that the ZTD assimilation improved the prediction of strong precipitation. Poli et al. (2007) also found a positive impact on the prediction of short-term precipitation and quantitative precipitation forecast scores for total precipitation over France between +12 and +36 h after analysis time. The Action de Recherche Petite Échelle Grande Échelle (ARPEGE) global model was used here to understand the assimilation impact of synoptic-scale circulations and precipitation forecasting during spring and summer. Yan et al. (2009) performed assimilation experiments using the Aire Limitée Adaptation dynamique Développement InterNational (ALADIN) model. They found that assimilating ZTDs improved the meso-nonhydrostatic precipitation forecasts for a heavy rainfall event over the Mediterranean region. Boniface et al. (2009) assimilated GNSS data into the Applications of Research to Operations at Mesoscale (AROME) model. They showed improvement in predicting the spatial extent of the precipitation. Lindskog et al. (2017) used the HIRLAM–ALADIN (High Resolution Limited Area Model; Aire Limitée Adaptation dynamique Développement InterNational) Research on Mesoscale Operational NWP in Euromed (HARMONIE) Applications of Research to Operations at Mesoscale (HARMONIE–AROME) model to test ZTD data assimilation (DA). Their findings show that including ZTD as an additional observation type enhances forecast accuracy, emphasizing the possibility of enhancing data assimilation by combining GNSS ZTD with other observations. Rohm et al. (2019) conducted assimilation studies using the Weather Research and Forecasting (WRF) model ZTD operator. They found that the ZTD assimilation altered the moisture field and precipitation rather than other parameters, such as the pressure or temperature field. GNSS observations enhance forecasts within 24 h, with the most impact at a 9 h lead time. Giannaros et al. (2020) and Caldas-Alvarez and Khodayar (2020) also demonstrated the significant benefits of incorporating GNSS ZTD data to improve precipitation and water vapor forecasts. Their studies used the WRF model in a broader Mediterranean region and the COSMO-CLM (COnsortium for Small-scale MOdeling in CLimate Mode) model in the central European region, respectively. Lagasio et al. (2019) discovered that integrating diverse Sentinel-1 and GNSS ZTD observations into the WRF model provides significant advantages for forecasts, offering detailed information on the wind field and water vapor content. Singh et al. (2019) found that using ZTD observations from a ground-based GNSS network improved humidity, air temperature, and wind forecasts in the Indian region. Assimilating these observations reduced forecast errors in wind fields and enhanced rainfall predictions to some extent. Mascitelli et al. (2019, 2021) successfully utilized the Regional Atmospheric Modeling System at the Institute of Atmospheric Sciences and Climate (RAMS@ISAC) model to incorporate GNSS ZTD data, leading to a significant enhancement in short-term water vapor prediction with minimal impact on precipitation forecasts. Yang et al. (2020) found that combining ZTD and radar data improved the accuracy of heavy rainfall location and intensity. They also discovered that using a broader horizontal localization scale instead of the convective scale for radar data assimilation enhanced the impact of ZTD data. Risanto et al. (2021) found that assimilating Global Positioning System (GPS) precipitable water vapor improved short-range North American monsoon precipitation forecasts by reducing errors and biases in the initial conditions of the weather model. This enhanced the model's ability to capture nocturnal convection of mesoscale convective systems and improved precipitation timing.

ZTDs are the only GNSS-derived moisture data used operationally; however, they provide limited atmospheric information. New observations must augment the existing observations, providing additional information. According to Bennitt and Jupp (2012) and Mahfouf et al. (2015), the limitations of ZTD lie in its inability to provide information on horizontal or vertical atmospheric gradients. Tropospheric gradient (TG) is another variable derived from the GNSS (Bar-Sever et al., 1998). In simple terms, TGs mainly provide information on the moisture's change (or "gradient") in a specific direction. Bar-Sever et al. (1998) showed that including TGs in GPS geodesy enhances accuracy and precision, with the estimated gradients matching real atmospheric moisture patterns observed by a water vapor radiometer (WVR). Walpersdorf et al. (2001) used the ALADIN model to validate GPS TGs at five stations. Iwabuchi et al. (2003) found a strong correlation between these gradients and moisture fields, with TGs typically pointing from dry to moist regions. Brenot et al. (2013) observed similar phenomena in their deep convection studies. Li et al. (2015) showed that better observation geometry improves gradient estimation accuracy. Morel et al. (2015) analyzed data from 12 Corsican stations using different software. Douša et al. (2016) analyzed data from hundreds of stations in central Europe and confirmed that GNSS TGs reflect real tropospheric features. Kačmařík et al. (2019) highlighted the sensitivity of TGs to processing options, emphasizing that real-time accuracy depends on high-quality satellite data.

Thundathil et al. (2024a) illustrate the operator implementation and assimilation of TGs in the WRF model. The TG operator (Zus et al., 2023) was incorporated into the WRF data assimilation (WRFDA) system in version 4.4.1. The source codes are published online for the research community worldwide. The study accomplished a 2-month assimilation impact study to obtain statistical confidence for the impact when focused on Europe. The observations for the impact studies were collected from the GFZ Helmholtz Centre for Geosciences. The study quantified the impact, showing promising improvements by adding TGs on top of ZTDs. In this study, we aim to further investigate the potential of TGs through a sensitivity experiment. We wish to analyze under which circumstances TGs provide information when combined with ZTDs to improve the initial conditions for numerical weather prediction.

2 GNSS ZTD and tropospheric gradients

The tropospheric delay is caused by the signal traveling through the neutral atmosphere. It is parameterized in the GNSS analysis with mapping functions (MFs), zenith delay, and gradient terms. The tropospheric delay T at the station is expressed as a function of the elevation angle e and the azimuth angle a:

$$\begin{aligned} T(e,a) = & m_{\mathrm{h}}(e)\, Z_{\mathrm{h}} + m_{\mathrm{w}}(e)\, Z_{\mathrm{w}} \\ & + m_{\mathrm{g}}(e)\left[\cos(a) N + \sin(a) E\right], \end{aligned} \tag{1}$$

where Z_{h} is the zenith hydrostatic delay (ZHD), Z_{w} is the zenith wet delay (ZWD), and N and E are the north and east gradient components. The hydrostatic, wet, and gradient MFs are denoted m_{h}, m_{w}, and m_{g}, respectively. The ZTD, Z, is given by

$$Z = Z_{\mathrm{h}} + Z_{\mathrm{w}}. \tag{2}$$

The forward operator for the ZTD, along with the tangent linear and adjoint operators, is already integrated into the WRFDA system. The ZTD is calculated through

$$Z = 10^{-6} \int \Psi \mathrm{d}z, \tag{3}$$

where the refractivity, Ψ, is a function of pressure, temperature, and humidity (Thayer, 1974), with z denoting the height above the station. In the GNSS data analysis, the ZTD (Z), the north gradient component (N), and the east gradient component (E) are estimated with geodetic parameters through least square adjustment (Gendt et al., 2004). The three quantities, depending on the state of the atmosphere in the vicinity of the station, are considered observations. The TG forward operator uses a fast approach which works as follows: for the given station location, we utilize a closed-form expression that depends on the north–south and east–west horizontal gradients of refractivity (as outlined in Davis et al., 1993). This enables the calculation of the north and east gradient components through

$$N = 10^{-6} \int z \Psi_y \mathrm{d}z, \tag{4}$$

$$E = 10^{-6} \int z \Psi_x \mathrm{d}z. \tag{5}$$

Here, x, y, and z represent the Cartesian coordinates, and partial derivatives are denoted by the corresponding subscripts. Similar to the computation of ZTDs, the TGs are also calculated using numerical integration.

Recently, Zus et al. (2023) developed the TG operator, which has been implemented into the WRFDA system version 4.4.1. Initial DA experiments conducted for the dense GNSS station network in Germany have shown promising results (Thundathil et al., 2024a). Additionally, Zus et al. (2025) introduced an open-source ray-tracing tool designed for space geodetic techniques. This software utilizes geometric optics to calculate the signal travel time delay caused by the atmosphere between two defined points.

3 Model setup

In this study, the WRF model version 4.4.1 is used with the Advanced Research WRF (ARW) core (Skamarock et al., 2008). WRF has been widely used for research within a large community and also serves as a model for operational forecasting at various agencies worldwide (Powers et al., 2017).

The model domain was configured with a 0.1° (approx. 11 km) horizontal resolution and 250 × 250 grid points. The number of vertical levels in the model is 50, extending from Earth's surface to an altitude of 50 hPa. The initial and boundary conditions were obtained from the European Centre for Medium-Range Weather Forecasts operational analysis, which had a spatial resolution of 0.14° (approx. 16 km). In this sensitivity study, we are using the GNSS observations from the "Benchmark dataset", which was collected within the European COST Action ES1206 GNSS4SWEC (Advanced GNSS tropospheric products for monitoring severe weather and climate; Douša et al., 2016). The GNSS stations in central Europe, covering Germany, the Czech Republic, and parts of Poland and Austria, provided the data during this campaign. Figure 1 shows the WRF model domain with the GNSS stations.

The WRF model physics settings are the same as those in Thundathil et al. (2024a). The radiation parameterization scheme used in this study is based on the Rapid Radiative Transfer Model for General Circulation Models (RRTMG) developed by Iacono et al. (2008). This model is recognized for its accuracy and efficiency in calculating long-wave and short-wave fluxes and heating rates, making it particularly suitable for applications in general circulation models.

For the cloud microphysics, we implemented the Thompson double-moment scheme (Thompson et al., 2008), which can predict mixing ratios for cloud water, rain, ice, snow,

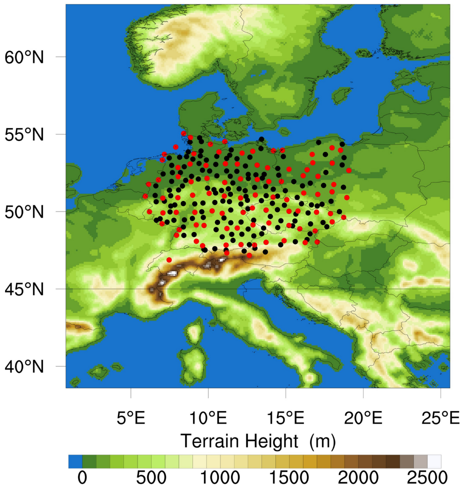

Figure 1. The WRF model domain with terrain height representation. The GNSS stations in the assimilation study are depicted in red to signify the sparse network with a 1° density, while the combination of black and red indicates the dense network with a 0.5° density.

and graupel. The planetary boundary layer scheme utilized in this simulation is the Yonsei University (YSU) scheme (Hong et al., 2010; Hong and Lim, 2006). The YSU is a non-local scheme with first-order closure that incorporates counter-gradient and explicit entrainment terms into the turbulence flux equation.

This study also employed the unified Noah land surface model (Chen and Dudhia, 2001). This model consists of four layers and is designed to predict soil temperature and moisture, canopy moisture, and snow cover. It takes into account various factors, including root zone dynamics, evapotranspiration, soil drainage, runoff, vegetation categories, and soil texture. This comprehensive approach yields valuable information on sensible and latent heat fluxes related to the boundary layer, including an enhanced treatment for urban areas.

To simulate the model accurately at a non-convective-scale resolution, it is crucial to include convection parameterization, which helps represent the statistical effects of sub-grid-scale convective clouds. For this purpose, we used the Grell–Freitas ensemble scheme (Grell and Freitas, 2014), which integrates a probability density function with data assimilation techniques.

3.1 Data

For the assimilation experiment, we had GNSS tropospheric products from 430 stations which belong to the core of the Benchmark dataset, which was collected within the European COST Action ES1206 GNSS4SWEC (Douša et al., 2016). The GNSS ZTDs and TGs were obtained in precise-point-positioning mode, utilizing the G-Nut/Tefnut software (Václavovic et al., 2014). Details on the quality of the tropospheric products can be found in Kačmařík et al. (2019). To ensure a homogeneous set of observations across the domain, we excluded colocated and clustered stations and specifically chose GNSS stations with data availability exceeding 75 %. In addition, to comply with our WRF model domain, we carried out a simple thinning of observations ("homogenization" of station distribution). The thinning method was conducted in two steps. First, a 0.5° mesh was constructed. Then, GNSS stations were selected based on their proximity to the mesh grid point. Finally, we obtained a station network with a resolution of about 0.5°. After these steps, we were left with around 250 GNSS stations over the Benchmark domain. For the sensitivity experiment, we created another thinned station network with a resolution of about 1° that contained around 110 stations (see Fig. 1). The same thinning procedure was used again. In line with the approach of Thundathil et al. (2024a), we intentionally excluded 18 stations in Germany from our dataset for validation purposes. These excluded stations were chosen strategically to maintain a balanced spatial distribution, aligning with the locations of the German Weather Service (DWD: Deutscher Wetterdienst) radar stations. The remaining stations included in the model are referred to as "allowed" stations. This method enabled us to analyze improvements with respect to independent observations. We utilized analyses from our control experiment to implement a "fixed" bias correction, addressing potential biases in the GNSS dataset (Thundathil et al., 2024a). The 2 months of simulation from the control experiment were employed to perform a station-specific bias correction for the GNSS ZTDs and TGs. The standard observation error for ZTDs in operational forecasting typically ranges from 5 to 15 mm. Similar to our previous study, Thundathil et al. (2024a), the same observation errors were adopted: 8 mm for the ZTDs and 0.65 mm for the TGs. Given the high quality of the observations from the Benchmark campaign dataset, we have maintained these same error values in this study. The north and east gradient observation errors were calculated based on an analysis of the observation-minus-background (OB) statistics from the control run. OB statistics encompass both observation and model errors. An observation error of 0.65 mm was conservative since we did not want to force the model too much to the observations. To improve the analysis, we assimilated a set of conventional observations in addition to the GNSS observations. The conventional observations included a network of surface stations (SYNOP) across Europe. Radiosonde measurements offered a detailed view of the atmospheric thermodynamic structure at launch points. In order to maintain simplicity within the DA system, we limited conventional datasets to SYNOP surface observations and radiosondes. The number of observations ranges from 1029 to 1225 for SYNOP stations and 4 to 35 for radiosondes.

3.2 DA framework

In this study, we used the deterministic three-dimensional variational (3DVAR) DA system. It uses an iterative minimization of the cost function J with a background constraint and an observation constraint. The 3DVAR cost function equation is given by

$$J(x) = \frac{1}{2}(x - x_b)^T \mathbf{B}^{-1}(x - x_b) + \frac{1}{2}(y - \mathbf{H}(x))^T \mathbf{R}^{-1}(y - \mathbf{H}(x)). \quad (6)$$

The variables x, x_b, and y are column vectors that represent the model state, the background (or first guess), and the observation state, respectively. The forward operator, denoted by $\mathbf{H}$, maps the model state vector to the observation vector. $\mathbf{B}$ represents the background error covariance matrix, while $\mathbf{R}$ represents the observation error covariance matrix. The observations are assumed to be uncorrelated, so $\mathbf{R}$ is a diagonal matrix. $\mathbf{B}$ is a square, positive, semi-definite, and symmetric matrix that contains the variances of the background forecast errors along the diagonal and their covariances in the upper and lower triangles of the matrix. We computed a climatological background error covariance matrix using the National Meteorological Center (NMC) method (Parrish and Derber, 1992). The NMC method involves calculating forecast difference statistics to obtain the forecast error covariance. The $\mathbf{B}$ matrix for the regional simulations was derived from the forecast statistics by analyzing differences in 24 and 12 h predictions over a month using data from May 2013. We chose the CV5 option for independent control of moisture levels, as it minimizes interference from other control variables. CV5 refers to a version of the background error covariance matrix used in the WRF model. It incorporates five control variables: stream function (Ψ), unbalanced velocity potential (χ_u), unbalanced temperature (T_u), pseudo-relative humidity ($\mathrm{RH_s}$), and unbalanced surface pressure ($P_\mathrm{s,u}$). Pseudo-relative humidity is the ratio of Q to $Q_\mathrm{b,s}$, where $Q_\mathrm{b,s}$ represents the saturated specific humidity of the background field.

The assimilation system used a 6-hourly DA cycle framework, with assimilations over May and June 2013. Spin-up is essential for the model to stabilize with the initial and boundary conditions, enabling it to respond accurately to any desired input. Only after a sufficient spin-up period can the model forecasts be considered reliable for further analysis through DA. For our study, we adopted a 12 h spin-up before the assimilation (Lauer et al., 2023). We conducted two sets of experiments. The first set comprised three experiments: (1) control run with assimilation of conventional data only, (2) ZTD run assimilating ZTDs on top of the control run, and (3) ZTDGRA run assimilating ZTDs and TGs on top of the control run. We term the second and third experiments ZTD_0.5° and ZTDGRA_0.5° to distinguish them from the second set of experiments, making them easier for readers to understand. In the 6-hourly DA cycle, an hourly forecast output was generated after each assimilation cycle for the next 5 h, which resulted in one analysis and five forecasts.

The second set of experiments was performed to analyze the sensitivity of the gradient observations by de-densification of the GNSS stations. We de-densified the GNSS stations from a roughly 0.5° to a 1° station network and then performed the assimilation experiments. Hence, ZTD_1.0° and ZTDGRA_1.0° runs were conducted similarly to ZTD_0.5° and ZTDGRA_0.5°, respectively, but with the assimilation of observations from the 1° station network. The assimilation cycle runs from 5 May 2013 00:00 UTC to 29 June 2013 18:00 UTC, i.e., the entire available data timeline from the Benchmark campaign. The DA framework of the experiments is shown in Fig. 2.

4 Results

4.1 Impact of GNSS data

To evaluate the impact of assimilating TGs on top of ZTDs, we conducted a comparative analysis of the results from 2-month-long assimilation experiments using data from GNSS stations. Specifically, we compared the analyses and forecasts obtained from these experiments against observations from GNSS stations, both assimilated and independent stations (which were not assimilated). The assimilated stations are termed as "allowed stations", and the independent stations are termed as "excluded stations", similar to Thundathil et al. (2024a). The quantitative comparison involved hourly GNSS station data, which were assessed against 6-hourly data assimilation (DA) analyses and 5 h forecasts initialized from these analyses. The model simulation for 2 months in each experiment comprises 6-hourly analyses and a 5 h forecast in between two DA cycles. Hence, the model simulations consist of hourly model outputs of analyses and forecasts. This hourly model output is compared to the corresponding GNSS station data for each experiment to calculate the root mean square error (RMSE). The model ZTDs and TGs at the locations of each specific station are computed for the RMSE. We term this the "station-specific RMSE". This section focuses on comparing the first set of experiments, labeled ZTD_0.5° and ZTDGRA_0.5°, with the control run.

Figure 3 is a simplified percentage analysis of the station-specific RMSE plot (please refer to Figs. A1–A6 in Appendix A for a more straightforward interpretation). Here, the control experiment was kept as the base experiment, and the ZTDs and ZTDs plus TGs assimilation experiments in dense and sparse configurations were compared. A reduction in the RMSEs indicates improvement in the assimilation experiment. The reduction in RMSE is represented as a percentage increase: the higher the reduction, the higher the percentage. Table 1 lists the average of the station-specific RMSEs of all the DA experiments for the 2 months. Figure 3 (top left) demonstrates that the ZTDGRA_0.5° experiment

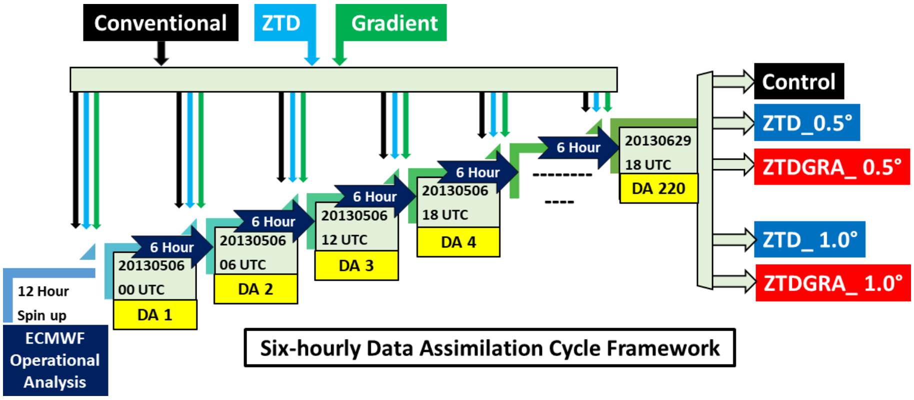

Figure 2. Schematic of the 3DVAR 6-hourly DA cycle initialized from the ECMWF operational analysis. Five experiments with different setups are performed in two sets. The first set comprises a control run assimilating conventional data, a ZTD_0.5° run assimilating ZTDs on top of the control run, and a ZTDGRA_0.5° run assimilating ZTD and TGs on top of the control run. These experiments are conducted with the observations from the (dense) 0.5° station network. The second set runs are ZTD_1_0° and ZTDGRA_1_0° with the assimilation of observations from the (sparse) 1° station network.

Table 1. Mean standard deviation derived from station-specific standard deviation. The allowed stations and the excluded stations are compared. The standard deviations, highlighted in bold, indicate that the values are similar for the ZTD dense network and the ZTDGRA sparse network.

Allowed stations						
Exp.	Standard deviation in mm (0.5°)			Standard deviation in mm (1.0°)		
	ZTD	N gradient	E gradient	ZTD	N gradient	E gradient
Control run	14.4	0.62	0.66	14.4	0.63	0.66
ZTD run	**8.3**	**0.52**	**0.54**	9.2	0.55	0.58
ZTDGRA run	8.2	0.49	0.5	**8.7**	**0.51**	**0.52**
Excluded stations						
Exp.	Standard deviation in mm (0.5°)			Standard deviation in mm (1.0°)		
	ZTD	N gradient	E gradient	ZTD	N gradient	E gradient
Control run	13.7	0.59	0.63	13.7	0.59	0.63
ZTD run	**8.2**	**0.49**	**0.51**	9	0.52	0.55
ZTDGRA run	8	0.47	0.48	**8.5**	**0.49**	**0.51**

yielded the lowest mean RMSE values for the ZTD parameter among all runs with the highest percentage reduction of 43 % in the mean station-specific RMSE with respect to the control run. This indicates the successful impact of gradient assimilation. Specifically, referring to Table 1, the mean RMSE for the ZTD variable decreased from 14.4 mm in the control run to 8.3 mm in the ZTD_0.5° run and further to 8.2 mm in the ZTDGRA_0.5° run. Improvements were observed not only in ZTD values but also in the gradient components. Both the north and east gradient components exhibited reductions in RMSE. For the north gradient, RMSE decreased from 0.62 mm in the control run to 0.52 mm in the ZTD_0.5° run and further to 0.49 mm in the ZTDGRA_0.5° run. Similarly, for the east gradient, RMSE decreased from 0.66 mm in the control run to 0.54 mm in the ZTD_0.5° run and then to 0.50 mm in the ZTDGRA_0.5° run. These reductions in RMSE values underscore the significant improvements achieved by assimilating TGs, which enhanced the moisture field representation in the model state. The findings highlight the synergistic relationship between ZTDs and TGs assimilation, where assimilating ZTDs contributes to the refinement of TG components, and vice versa.

To confirm that these improvements were not solely due to comparisons with observations from the assimilated GNSS stations, we extended the analysis to include 18 independent GNSS stations that were excluded from the assimilation process. Again the highest RMSE reduction of 42 % was observed in the ZTDGRA_0.5° run compared to the control run. The RMSE for the ZTD variable decreased from 13.7 mm in the control run to 8.2 mm in the ZTD_0.5° run

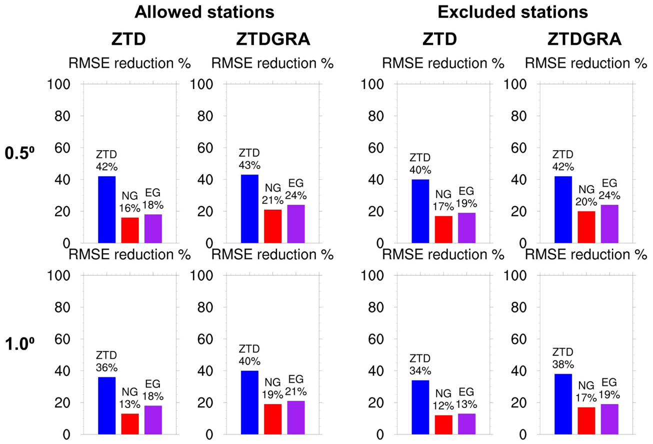

Figure 3. RMSE comparison w.r.t stations: assimilated or "allowed" and independent or "excluded". The plot shows the RMSE reduction w.r.t the control run in percentage. The gradient components are termed NG for the north gradient and EG for the east gradient. Please refer to Appendix A for a detailed plot.

and further to 8.0 mm in the ZTDGRA_0.5° run (Table 1). Similar trends were observed for the gradient components. For the north gradient, RMSE decreased from 0.59 mm in the control run to 0.49 mm in the ZTD_0.5° run and 0.47 mm in the ZTDGRA_0.5° run. For the east gradient, RMSE reduced from 0.63 mm in the control run to 0.51 mm in the ZTD_0.5° run and then to 0.48 mm in the ZTDGRA_0.5° run.

These consistent results across both assimilated and independent GNSS station data demonstrate the robust improvements achieved through gradient assimilation on top of ZTDs. The 2-month-long statistical evaluation confirms that the combined assimilation of ZTDs and TGs improves the humidity field.

To quantify the relative impact of GNSS observations compared to other point observations in the study (specifically the SYNOP station data), we utilized the Desroziers method. The Desroziers method is an effective diagnostic tool used to evaluate the impact of various observations. By analyzing the innovation (observation minus background, OMB) and residual (observation minus analysis, OMA) statistics, we can estimate the covariances of observation and background errors. This analysis helps us determine the relative influence of different types of observations on the overall analysis.

The relative impact of an observation is determined by the ratio of the estimated observation error covariance **R** to the estimated background error covariance **B**. The respective error covariances are calculated as below:

$$\mathbf{R} = E\left[(y - Hx^{\mathrm{a}})(y - Hx^{\mathrm{a}})^{T}\right], \tag{7}$$

$$\mathbf{B} = E\left[(y - Hx^{\mathrm{b}})(y - Hx^{\mathrm{a}})^{T}\right]. \tag{8}$$

Here $(y - Hx^{\mathrm{b}})$ is the innovation and $(y - Hx^{\mathrm{a}})$ is the residual, where x^{a}, x^{b}, and y are the model state vectors for analysis, background, and observations, respectively.

The higher the value of the ratio $\mathbf{B}/\mathbf{R}$, the higher the impact of the observation. The observations likely to enhance the model or lead to effective assimilation fall within the range of 0.5 to 3. A value below 0.5 suggests that the observation has a large error, making it unreliable for assimilation. Conversely, values above 3 indicate that the observation forces the background towards the observation, which may result from a small observation error or a bias in the observation. After analyzing 220 DA cycles, the average $\mathbf{B}/\mathbf{R}$ ratios were as follows: SYNOP at 1.4, ZTD at 2.8, NG at 1.8, and EG at 1.5. These values indicate that the impacts of the observations are well within the acceptable range. Additionally, TGs, have an impact on the assimilation system. The north and east gradient values indicate that the assimilation was effective. The ZTD observation has higher values, which might indicate that the observation error assigned to ZTDs could be higher than the current observation error value of 8 mm.

4.2 Sensitivity analysis

A sensitivity experiment was conducted to better understand the conditions under which the assimilation of TGs, in addition to ZTDs, improves the representation of the humidity field. For this purpose, a second set of experiments was designed using GNSS data assimilation from a sparser 1° network. This allowed for a focused analysis of the additional impact brought by gradient assimilation. As with the dense-network experiments, two configurations were tested: a ZTD assimilation run (ZTD_1.0°) and a combined assimilation run incorporating both ZTDs and TGs (ZTDGRA_1.0°).

When comparing data from stations included in the assimilation process, the ZTDGRA_1.0° experiment exhibited the lowest mean RMSE values for ZTD, similar to the results observed with the dense-network configuration. The highest reduction was 42 % for the ZTDGRA_1.0° run. Specifically, referring to Table 1, the ZTD variable's mean RMSE decreased from 14.4 mm in the control run to 9.2 mm in the ZTD_1.0° run and further to 8.7 mm in the ZTDGRA_1.0° run. For the TGs, RMSE values showed improvements in both the north and east components. The north gradient RMSE reduced from 0.63 mm in the control run to 0.55 mm in the ZTD_1.0° run and to 0.51 mm in the ZTDGRA_1.0° run. Similarly, the east gradient RMSE decreased from 0.66 mm in the control run to 0.58 mm in the ZTD_1.0° run and further to 0.52 mm in the ZTDGRA_1.0° run.

A comparable trend was observed with data from 18 independent GNSS stations excluded from the assimilation. For these stations, the ZTD variable's mean RMSE decreased from 13.7 mm in the control run to 9.0 mm in the ZTD_1.0° run and further to 8.5 mm in the ZTDGRA_1.0° run, which was a reduction of 38 % in ZTDGRA_1.0° from 34 % in the ZTD_1.0° run. The north gradient RMSE dropped from

0.59 mm in the control run to 0.52 mm in the ZTD_1.0° run and to 0.49 mm in the ZTDGRA_1.0° run (Table 1). Similarly, the east gradient RMSE declined from 0.63 mm in the control run to 0.55 mm in the ZTD_1.0° run and further to 0.51 mm in the ZTDGRA_1.0° run.

From the RMSE values, we conclude that, particularly for a sparse-network configuration, we can expect a significant impact on the assimilation of TGs on top of ZTDs. For example, suppose we utilize the RMSE of ZTDs for the independent stations as an indication of the improvement in the (integrated) water vapor field. In that case, referring to Table 1, the drop in the RMSE from 8.2 mm in the ZTD_0.5° experiment to 8.0 mm in the ZTDGRA_0.5° experiment is smaller than the drop from 9.0 mm in the ZTD_1.0° experiment to 8.5 mm in the ZTDGRA_1.0° experiment. A similar trend can be seen when we utilize the RMSE of ZTDs for the "allowed" stations.

The most striking feature was that the RMSE reduction of the ZTDGRA_1.0° run was similar to the ZTD_0.5° run. In other words, the assimilation of ZTDs and TGs from a sparse station network performed equally well as that of only ZTDs from the dense station network. In order to illustrate this visually, the analysis increments of ZTDGRA_1.0° and ZTD_0.5° runs for consecutive DA cycles were analyzed. Figure 4 shows five analysis increments from the first DA cycle on 6 May 2013 00:00 UTC until 7 May 2013 00:00 UTC, with assimilation every 6 h. Figure 4 is a zoomed-in map that covers only the countries where the GNSS stations were located. The rows in the plot refer to the corresponding DA cycles with ZTDGRA_1.0° on the left column and ZTD_0.5° on the right. DA cycle 1 refers to Fig. 4a and f, and DA cycles 2, 3, 4, and 5 refer to Fig. 4b and g, c and h, d and i, and e and j, respectively. The water vapor mixing ratio over the domain is vertically averaged for the first 16 model levels to portray the impact from the surface level up to the lower troposphere (approx. 6 km height). From the analysis increment comparison, a close match was observed between the two experiments with respect to respective assimilation cycles. From a visual inspection of the plots, the sparse-network assimilation of ZTD and gradient run had the same structures as seen in the dense-network assimilation of the ZTD alone run. Quantitatively, the similarity of the ZTD_0.5° and ZTDGRA_1.0° runs at respective assimilation cycles can be computed by the structural similarity (SSIM) index parameter. The SSIM (Wang et al., 2004) is a metric used to quantify the similarity between two images. The value ranges from 0 to 1 where 0 shows no similarity and 1 shows a perfect similarity. Here is a short explanation of the computation of SSIM in our study:

$$\mathrm{SSIM}(A,B)=\frac{(2\mu_A\mu_B+c_1)(2\sigma_{AB}+c_2)}{(\mu_A^2+\mu_B^2+c_1)(\sigma_A^2+\sigma_B^2+c_2)} \tag{9}$$

Here A and B represent the images in the left column (ZTDGRA_1.0°) and the right column (ZTD_0.5°), respectively. Water vapor mixing ratio (WVMR) is the moisture variable presented here in the images with a span of 101 colors. μ_A and μ_B are the means, σ_A^2 and σ_B^2 are the variances, and σ_{AB} is the covariance. The variables c_1 and c_2 are computed based on the color span in the images.

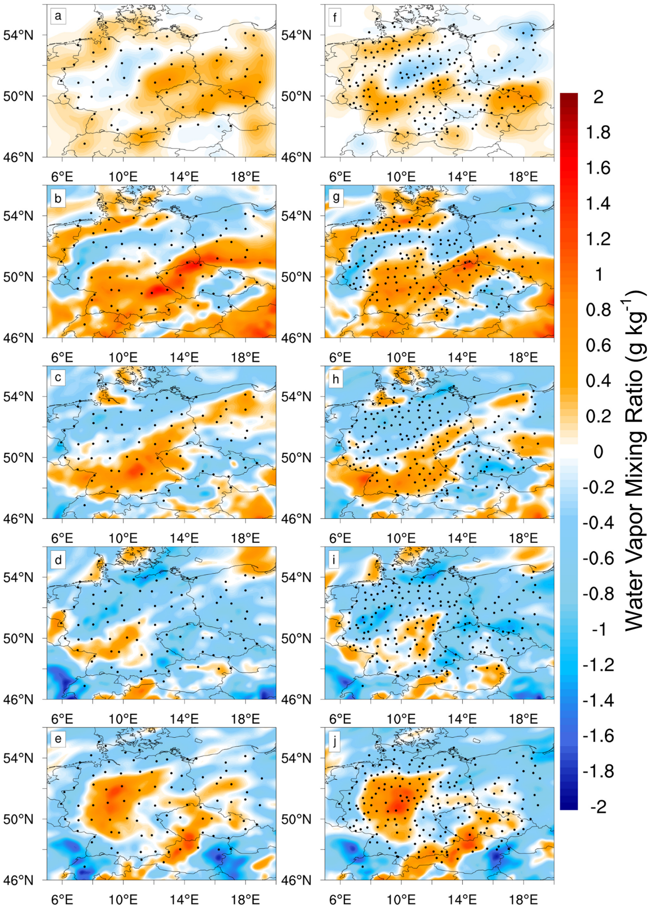

Figure 4. Spatial comparison of the evolution of the analysis increments of ZTDGRA_1.0° **(a–e)** and ZTD_0.5° **(f–j)** runs for the first five assimilation cycles. The stations used for the respective assimilation runs are depicted by black dots.

$$c_1=(k_1L)^2 \tag{10}$$

$$c_2=(k_2L)^2 \tag{11}$$

Here k_1 and k_2 are 0.01 and 0.03 by default. L here is the total number of colors in the color bar minus one. Hence, the values of c_1 and c_2 come to 1 and 3. Here, we computed the SSIM at all five assimilation cycles, showing a considerable similarity of the SSIM index greater than 0.98.

Finally, we took a closer look at the background and analyzed humidity profiles. In order to analyze the humidity profile correction in the assimilation experiment, we computed the RMSE of specific humidity profiles from model simulations with respect to ERA5 (Hersbach et al., 2020) at five locations spread equidistantly across the domain (for details, see Thundathil et al., 2024a). The RMSE of the pro-

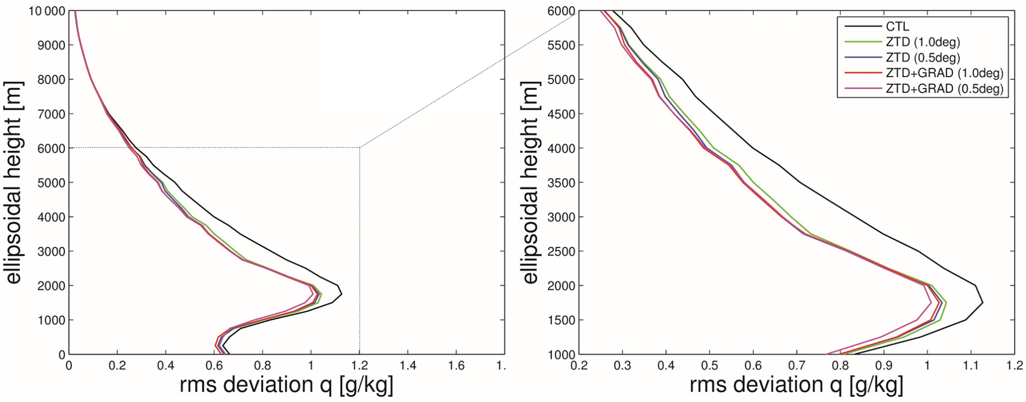

Figure 5. The RMSE of specific humidity profiles compared to ERA5 for control run (black), ZTD_0.5° run (blue), ZTD_1.0° run (green), ZTDGRA_1.0° run (red), and ZTDGRA_0.5° run (purple). Profiles were compared at five selected stations for 220 DA cycles, totaling 1100 profiles for the average plot.

files with respect to ERA5 averaged over the 2 months is shown in Fig. 5. There were 220 DA cycles, and with five profile RMSE comparisons at each cycle; the number of profiles totaled 1100. From the figure, the RMSE of the ZTDGRA_1.0° run appears to overlap with the ZTD_0.5° run. This shows that the information passed into the model when TGs are assimilated on top of ZTDs for sparse-network configurations is roughly as effective as the assimilation of ZTDs from the dense-network configuration. This finding is particularly relevant for those aiming to densify their existing GNSS networks for weather prediction purposes. Before the costly installation and maintenance of additional (single- or dual-frequency) GNSS stations, one should consider the assimilation of TGs on top of the ZTDs.

4.3 Forecast impact

To understand how long the effects of GNSS observation assimilations persist within the model, we conducted simulations of 24 h forecasts based on a 3 d analysis. Each day included four assimilation cycles, resulting in a total of 12 forecasts, each covering 24 h. The forecast is better validated with independent observations that are not assimilated into the model. With the 18 excluded GNSS stations, we can directly compare the model forecast with observations from the GNSS stations. Figure 6 compares the 12-forecast average with the GNSS ZTDs and TGs, including the north and east gradients, to compute the standard deviation. We analyzed three impact experiments: ZTD_1.0°, ZTD_0.5°, and ZTDGRA_1.0°, in addition to the control run. As anticipated, the effects of the three impact experiments gradually diminish and converge with the control run. If we define the endpoint of the impact as the moment when the standard deviation of the impact experiment aligns with that of the control run, then the duration of the impact is 12 h. The effects of the assimilation last for no more than 12 h, which is quite reasonable for moisture data assimilation. Additionally, it is important to note that incorporating TGs along with ZTDs enhances the forecast. Furthermore, the forecast impact of ZTDGRA_1.0° is comparable to that of ZTD_0.5°.

5 Conclusions

The TGs contain valuable information that has yet to be fully utilized by numerical weather models. From the assimilation experiments, we conclude that TGs, when assimilated in addition to ZTDs, enhance the accuracy of the humidity fields, thereby increasing the forecast accuracy. The work by Thundathil et al. (2024a) already provided evidence that gradient observations positively impacted the analyses and forecast. The important result of this paper is the dependency of the impact of gradient observations on the network configuration. Since TGs can be roughly related to horizontal ZTD gradients, it was hypothesized that the impact of this new observation type would be beneficial, particularly for a sparse-network configuration (Zus et al., 2019). Our results utilizing the state-of-the-art data assimilation system of WRF and GNSS tropospheric products from the Benchmark campaign prove this to be the case.

GNSS stations are available worldwide, but the station density varies from place to place. For example, the dense GNSS station network in Europe, with its near real-time data provision capability, is already in its current status very effective at filling gaps in the humidity fields required for operational weather forecasting. However, in regions with a sparse GNSS station network or remote regions with isolated GNSS stations, the provided ZTD data leave significant gaps in the highly variable humidity field. These gaps can be filled utilizing TGs.

Numerical weather models will run globally at high resolution in the near future. For instance, ECMWF's global operational forecast already has a resolution of 9 km. In the future, we will also have convection-scale resolution models

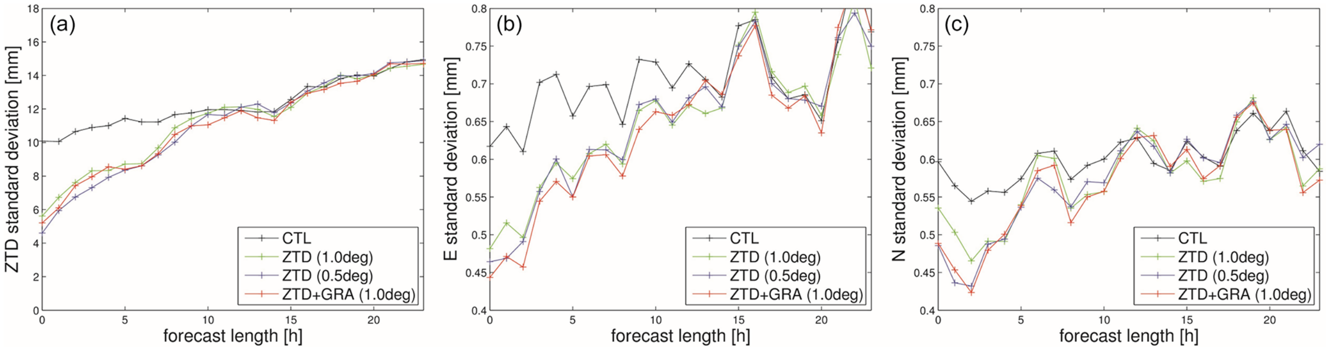

Figure 6. Average forecast impact with a 24 h lead time initiated from 12 analyses over 3 d starting from 6 May 2013 00:00 UTC. The control run (black), ZTD_1.0° run (green), ZTD_0.5° run (blue), and ZTDGRA_1.0° run (red) forecasts are compared to independent GNSS stations. **(a)** ZTD standard deviation; **(b)** east gradient standard deviation; **(c)** north gradient standard deviation.

running on a global scale, which would demand more observations for their initialization. We expect that the assimilation of GNSS TGs, in addition to ZTDs, helps to close gaps in the knowledge of the humidity field.

Appendix A

A detailed analysis of the assimilation impact of the GNSS data products is depicted through additional figures. The six figures and the table in this section provide supporting information on how Fig. 3 in the main article was derived. The specific impacts of the assimilation due to ZTDs and TGs with both dense and sparse assimilation setups are shown through the standard deviation compared to each GNSS station. The statistics were derived using the analysis and compared to the assimilated GNSS stations and independent GNSS stations, which were excluded from the assimilation dataset. We term the assimilated stations “Allowed” and the independent stations “Excluded.” Please refer the Figs. A1–A6. Additionally, Table 1 summarizes all the mean values of the standard deviation for all experiments to give a general overview of the impact of assimilation.

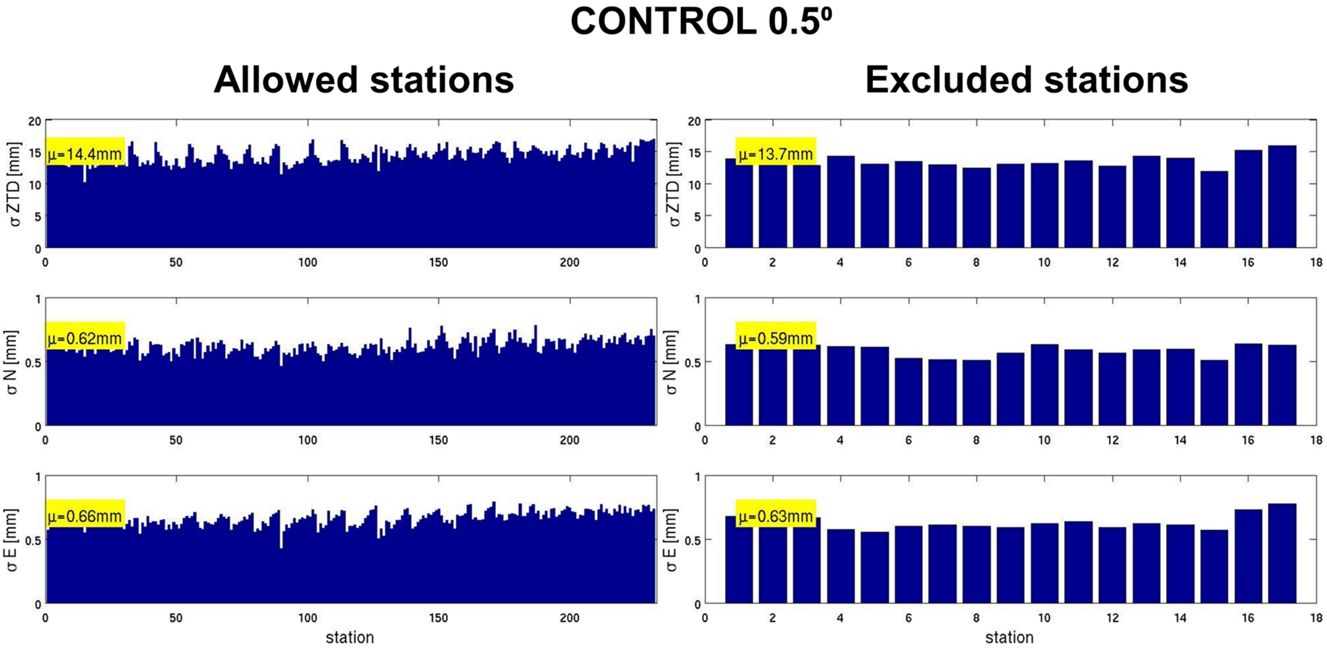

Figure A1. Station-specific standard deviation of the control run with dense-network configuration. ZTD, north gradient, and east gradient are shown for the allowed and excluded stations on the left column and right column, respectively. The mean values are shown as text with yellow background.

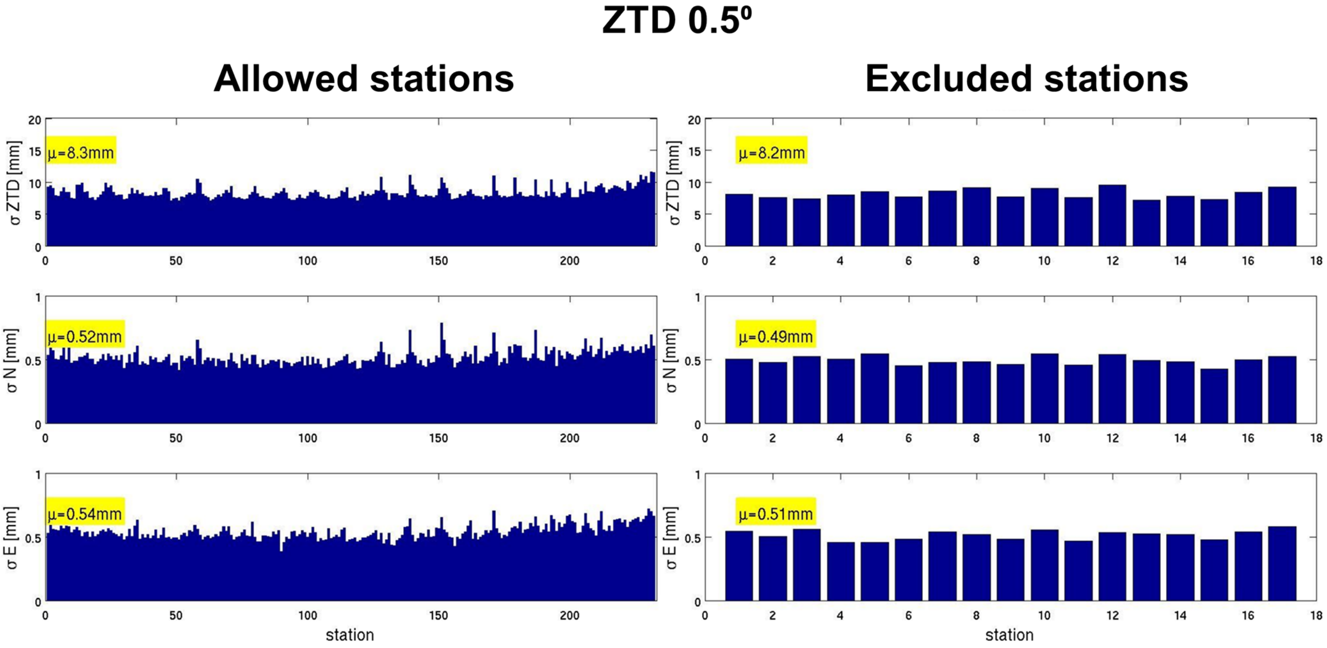

Figure A2. Same as Fig. A1 but for ZTD run in the dense-network configuration.

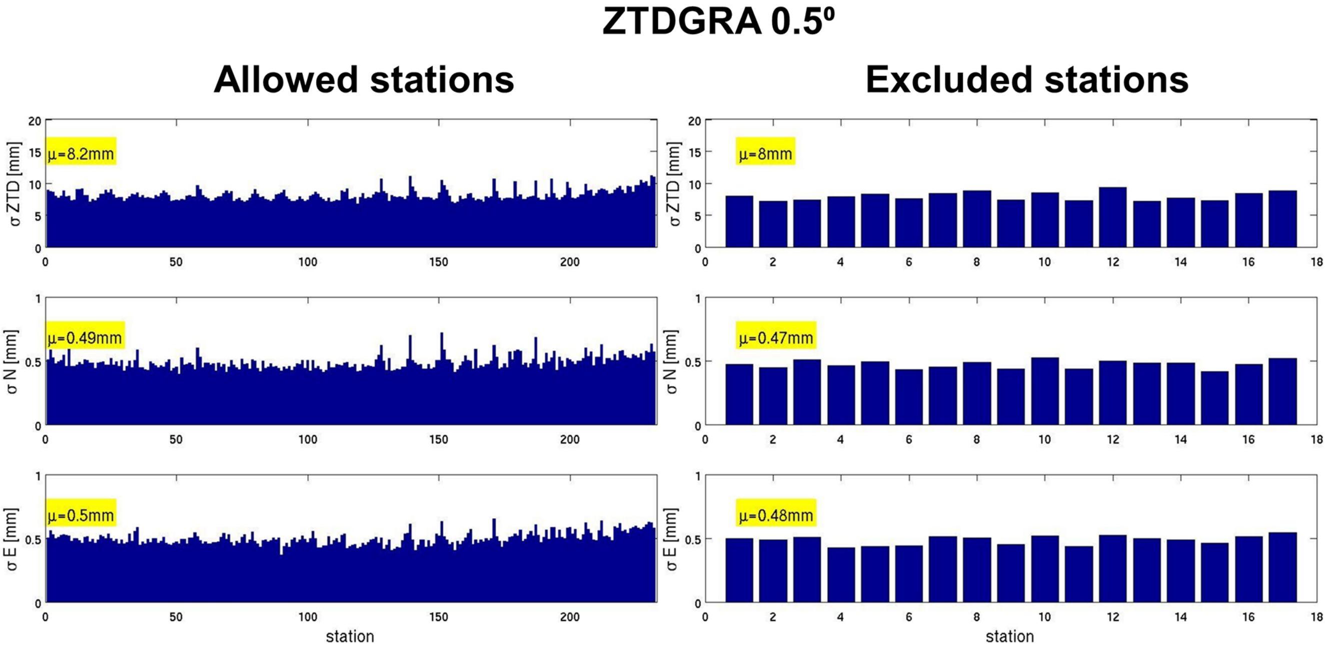

Figure A3. Same as Fig. A1 but for ZTDGRA run in the dense-network configuration.

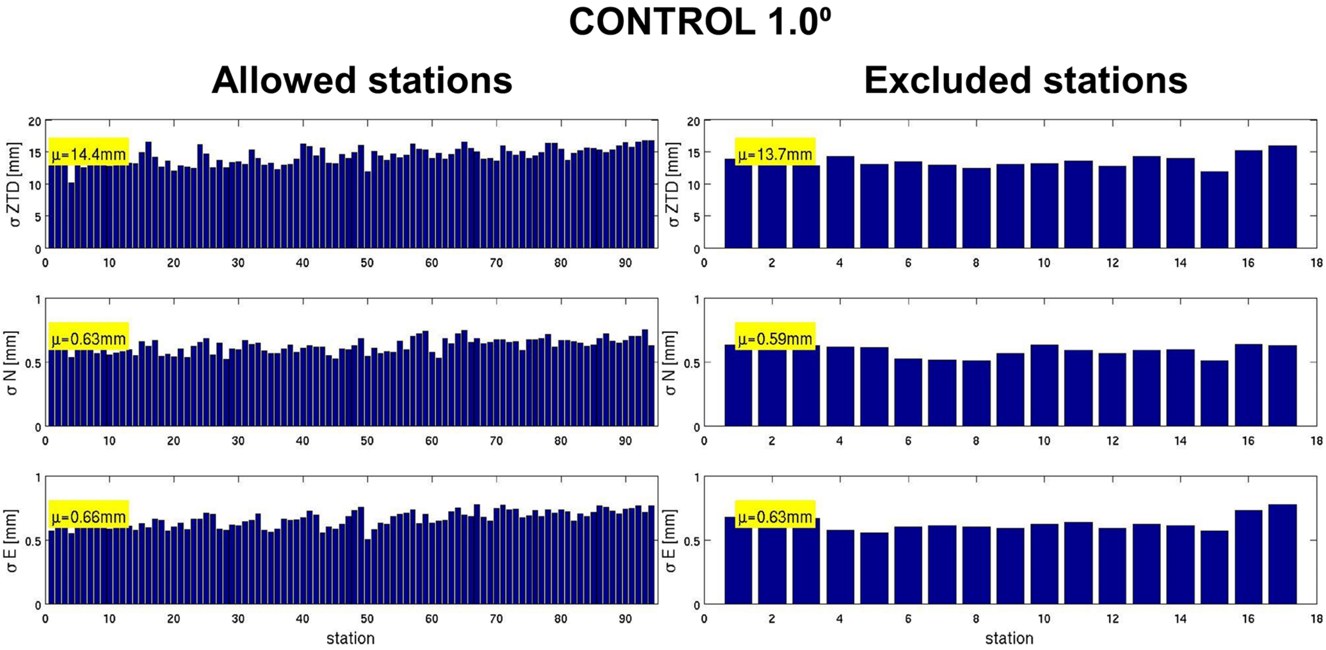

Figure A4. Same as Fig. A1 but for control run in the sparse-network configuration.

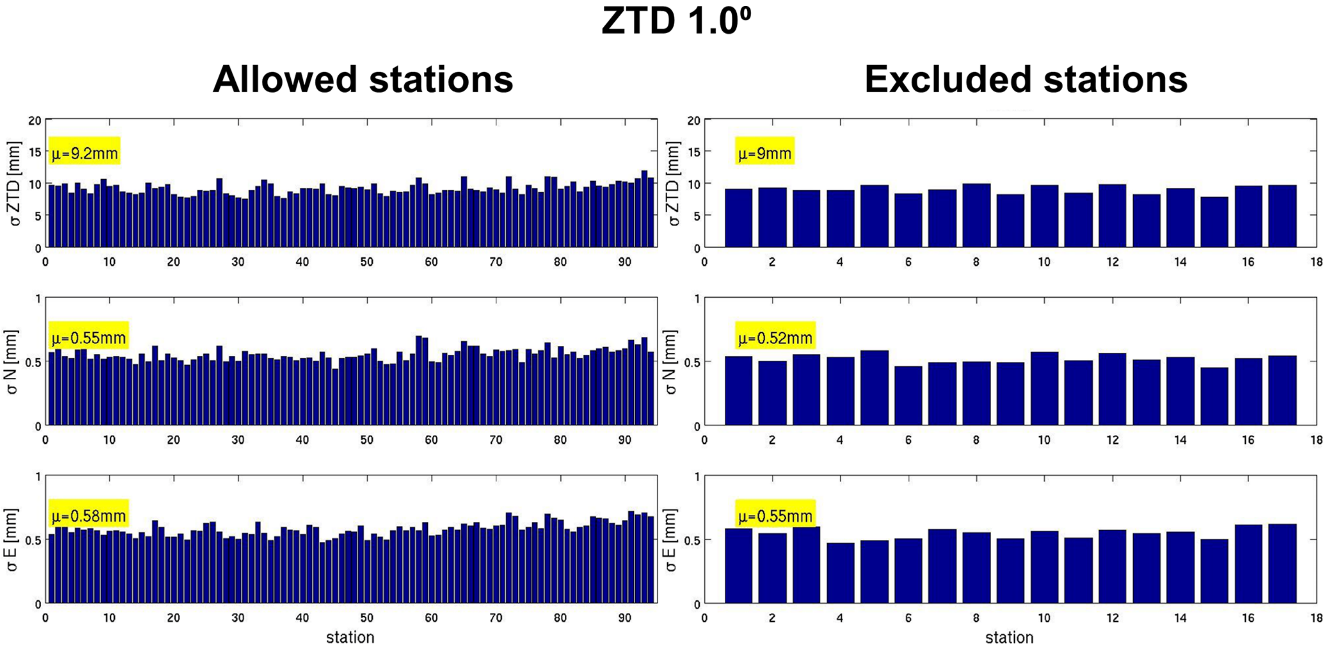

Figure A5. Same as Fig. A1 but for ZTD run in the sparse-network configuration.

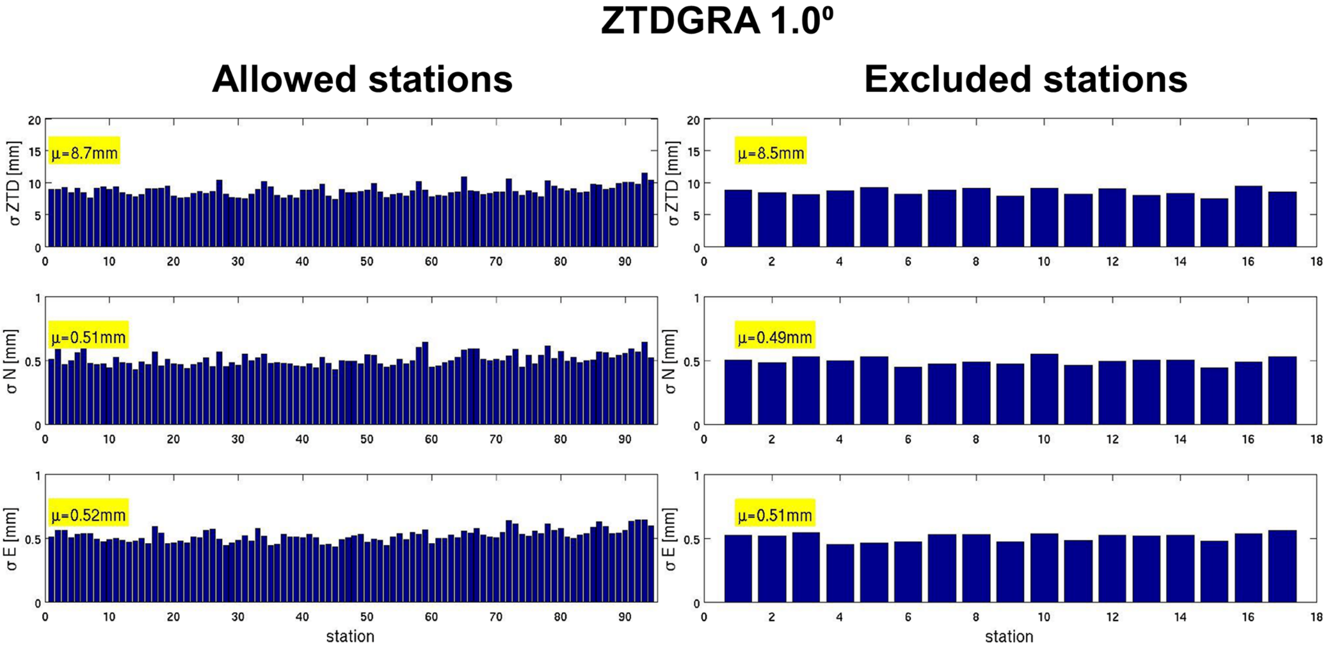

Figure A6. Same as Fig. A1 but for ZTDGRA run in the sparse-network configuration.

Code and data availability. The model simulation data and the WRFDA code version 4.4.1, with the gradient operator codes, are available for download. They are stored on Zenodo, a general-purpose open repository developed under the European Open-Access Infrastructure for Research in Europe (OpenAIRE) program and operated by the European Organization for Nuclear Research (CERN). The access link is https://doi.org/10.5281/zenodo.13734634 (Thundathil et al., 2024b). The GNSS data used for the research study were provided by the Geodetic Observatory Pecny (GOP) (http://www.pecny.cz, last access: 25 February 2023).

Author contributions. The original draft of the study was written by RT, who also conducted the formal analysis and experiments. FZ and RT collaborated to modify the WRFDA code and develop the gradient operator. JW and GD supervised the project, acquired funding, and reviewed and edited the paper.

Competing interests. The contact author has declared that none of the authors has any competing interests.

Acknowledgements. The research project is funded by the German Research Foundation (DFG; grant no. 68510200) and is titled "Exploitation of GNSS tropospheric gradients for severe weather Monitoring And Prediction (EGMAP)". The ECMWF conventional datasets for the DA study in this research were provided by Thomas Schwitalla from our collaborative institution, the Institute of Physics and Meteorology, University of Hohenheim, Stuttgart. The GNSS data were provided in a user-friendly format by Michal Kačmařík, who was working at Geodetic Observatory Pecny (GOP) during the European COST Action ES1206 project.

Financial support. This research has been supported by the Deutsche Forschungsgemeinschaft (grant no. 68510200).

The publication of this article was funded by the Open Access Publication Fund of TU Berlin.

Review statement. This paper was edited by Roeland Van Malderen and reviewed by four anonymous referees.

References

Bar-Sever, Y. E., Kroger, P. M., and Borjesson, J. A.: Estimating horizontal gradients of tropospheric path delay with a single GPS receiver, J. Geophys. Res.-Sol. Ea., 103, 5019–5035, https://doi.org/10.1029/97JB03534, 1998.

Bennitt, G. V. and Jupp, A.: Operational assimilation of GPS zenith total delay observations into the Met Office numerical weather prediction models, Mon. Weather Rev., 140, 2706–2719, https://doi.org/10.1175/MWR-D-11-00156.1, 2012.

Bevis, M., Businger, S., Herring, T. A., Rocken, C., Anthes, R. A., and Ware, R. H.: GPS meteorology: Remote sensing of atmospheric water vapor using the global positioning system, J. Geophys. Res.-Atmos., 97, 15787–15801, https://doi.org/10.1029/92JD01517, 1992.

Boniface, K., Ducrocq, V., Jaubert, G., Yan, X., Brousseau, P., Masson, F., Champollion, C., Chéry, J., and Doerflinger, E.: Impact of high-resolution data assimilation of GPS zenith delay on Mediterranean heavy rainfall forecasting, Ann. Geophys., 27, 2739–2753, https://doi.org/10.5194/angeo-27-2739-2009, 2009.

Brenot, H., Neméghaire, J., Delobbe, L., Clerbaux, N., De Meutter, P., Deckmyn, A., Delcloo, A., Frappez, L., and Van Roozendael, M.: Preliminary signs of the initiation of deep convection by GNSS, Atmos. Chem. Phys., 13, 5425–5449, https://doi.org/10.5194/acp-13-5425-2013, 2013.

Caldas-Alvarez, A. and Khodayar, S.: Assessing atmospheric moisture effects on heavy precipitation during HyMeX IOP16 using GPS nudging and dynamical downscaling, Nat. Hazards Earth Syst. Sci., 20, 2753–2776, https://doi.org/10.5194/nhess-20-2753-2020, 2020.

Chen, F. and Dudhia, J.: Coupling an advanced land surface-hydrology model with the Penn State–NCAR MM5 modeling system. Part I: Model implementation and sensitivity, Mon. Weather Rev., 129, 569–585, https://doi.org/10.1175/1520-0493(2001)129<0569:CAALSH>2.0.CO;2, 2001.

Davis, J. L., Elgered, G., Niell, A. E., and Kuehn, C. E.: Ground-based measurement of gradients in the "wet" radio refractivity of air, Radio Sci., 28, 1003–1018, https://doi.org/10.1029/93RS01917, 1993.

Douša, J., Dick, G., Kačmařík, M., Brožková, R., Zus, F., Brenot, H., Stoycheva, A., Möller, G., and Kaplon, J.: Benchmark campaign and case study episode in central Europe for development and assessment of advanced GNSS tropospheric models and products, Atmos. Meas. Tech., 9, 2989–3008, https://doi.org/10.5194/amt-9-2989-2016, 2016.

Gendt, G., Dick, G., Reigber, C., Tomassini, M., Liu, Y., and Ramatschi, M.: Near real time GPS water vapor monitoring for numerical weather prediction in Germany, J. Meteorol. Soc. Jpn. Ser. II, 82, 361–370, https://doi.org/10.2151/jmsj.2004.361, 2004.

Giannaros, C., Kotroni, V., Lagouvardos, K., Giannaros, T. M., and Pikridas, C.: Assessing the impact of GNSS ZTD data assimilation into the WRF modeling system during high-impact rainfall events over Greece, Remote Sens., 12, 383, https://doi.org/10.3390/rs12030383, 2020.

Hersbach, H., Bell, B., Berrisford, P., Hirahara, S., Horányi, A., Muñoz-Sabater, J., Nicolas, J., Peubey, C., Radu, R., Schepers, D., Simmons, A., Soci, C., Abdalla, S., Abellan, X., Balsamo, G., Bechtold, P., Biavati, G., Bidlot, J., Bonavita, M., De Chiara, G., Dahlgren, P., Dee, D., Diamantakis, M., Dragani, R., Flemming, J., Forbes, R., Fuentes, M., Geer, A., Haimberger, L., Healy, S., Hogan, R. J., Hólm, E., Janisková, M., Keeley, S., Laloyaux, P., Lopez, P., Lupu, C., Radnoti, G., de Rosnay, P., Rozum, I., Vamborg, F., Villaume, S., and Thépaut, J. N.: The ERA5 global reanalysis, Q. J. Roy. Meteor. Soc., 146, 1999–2049, https://doi.org/10.1002/qj.3803, 2020.

Grell, G. A. and Freitas, S. R.: A scale and aerosol aware stochastic convective parameterization for weather and air quality modeling, Atmos. Chem. Phys., 14, 5233–5250, https://doi.org/10.5194/acp-14-5233-2014, 2014.

Hong, S.-Y. and Lim, J.-O. J.: The WRF single-moment 6-class microphysics scheme (WSM6), Asia-Pac. J. Atmos. Sci., 42, 129–151, https://www.dbpia.co.kr/journal/articleDetail?nodeId=node00937254 (last access: 25 September 2025), 2006.

Hong, S.-Y., Lim, K.-S. S., Lee, Y.-H., Ha, J.-C., Kim, H.-W., Ham, S.-J., and Dudhia, J.: Evaluation of the WRF double-moment 6-class microphysics scheme for precipitating convection, Adv. Meteorol., 2010, 707253, https://doi.org/10.1155/2010/707253, 2010.

Iacono, M. J., Delamere, J. S., Mlawer, E. J., Shephard, M. W., Clough, S. A., and Collins, W. D.: Radiative forcing by long-lived greenhouse gases: Calculations with the AER radiative transfer models, J. Geophys. Res.-Atmos., 113, D13103, https://doi.org/10.1029/2008JD009944, 2008.

Iwabuchi, T., Miyazaki, S. I., Heki, K., Naito, I., and Hatanaka, Y.: An impact of estimating tropospheric delay gradients on tropospheric delay estimations in the summer using the Japanese nationwide GPS array, J. Geophys. Res.-Atmos., 108, https://doi.org/10.1029/2002JD002214, 2003.

Kačmařík, M., Douša, J., Zus, F., Václavovic, P., Balidakis, K., Dick, G., and Wickert, J.: Sensitivity of GNSS tropospheric gradients to processing options, Ann. Geophys., 37, 429–446, https://doi.org/10.5194/angeo-37-429-2019, 2019.

Lagasio, M., Pulvirenti, L., Parodi, A., Boni, G., Pierdicca, N., Venuti, G., Realini, E., Tagliaferro, G., Barindelli S., and Rommen, B.: Effect of the ingestion in the WRF model of different Sentinel-derived and GNSS-derived products: analysis of the forecasts of a high impact weather event, Eur. J. Remote Sens., 52, 16–33, https://doi.org/10.1080/22797254.2019.1642799, 2019.

Lauer, A., Devaney, J., Kieu, C., Kravitz, B., O'Brien, T. A., Robeson, S. M., Staten, P. W., and Vu, T. A.: A convection-permitting dynamically downscaled dataset over the Midwestern United States, Geosci. Data J., 10, 429–446, https://doi.org/10.1002/gdj3.188, 2023.

Li, X., Zus, F., Lu, C., Ning, T., Dick, G., Ge, M., Wickert, J., and Schuh, H.: Retrieving high-resolution tropospheric gradients from multiconstellation GNSS observations, Geophys. Res. Lett., 42, 4173–4181, https://doi.org/10.1002/2015GL063856, 2015.

Lindskog, M., Ridal, M., Thorsteinsson, S., and Ning, T.: Data assimilation of GNSS zenith total delays from a Nordic processing centre, Atmos. Chem. Phys., 17, 13983–13998, https://doi.org/10.5194/acp-17-13983-2017, 2017.

Mahfouf, J. F., Ahmed, F., Moll, P., and Teferle, F. N.: Assimilation of zenith total delays in the AROME France convective scale model: a recent assessment, Tellus A, 67, 26106, https://doi.org/10.3402/tellusa.v67.26106, 2015.

Mascitelli, A., Federico, S., Fortunato, M., Avolio, E., Torcasio, R. C., Realini, E., Mazzoni, A., Transerici, C., Crespi, M., and Dietrich, S.: Data assimilation of GPS-ZTD into the RAMS model through 3D-Var: preliminary results at the regional scale, Meas. Sci. Technol., 30, 055801, https://doi.org/10.1088/1361-6501/ab0b87, 2019.

Mascitelli, A., Federico, S., Torcasio, R. C., and Dietrich, S.: Assimilation of GPS Zenith Total Delay estimates in RAMS NWP model: Impact studies over central Italy, Adv. Space Res., 68, 4783–4793, https://doi.org/10.1016/j.asr.2020.08.031, 2021.

Morel, L., Pottiaux, E., Durand, F., Fund, F., Boniface, K., de Oliveira Junior, P. S., and Van Baelen, J.: Validity and behaviour of TGs estimated by GPS in Corsica, Adv. Space Res., 55, 135–149, https://doi.org/10.1016/j.asr.2014.10.004, 2015.

Parrish, D. F. and Derber, J. C.: The National Meteorological Center's spectral statistical-interpolation analysis system, Mon. Weather Rev., 120, 1747–1763, https://repository.library.noaa.gov/view/noaa/11449 (last access: 23 September 2025), 1992.

Poli, P., Moll, P., Rabier, F., Desroziers, G., Chapnik, B., Berre, L., Healy, S. B., Andersson, E., and El Guelai, F. Z.: Forecast impact studies of zenith total delay data from European near real-time GPS stations in Météo France 4DVAR, J. Geophys. Res.-Atmos., 112, https://doi.org/10.1029/2006JD007430, 2007.

Powers, J. G., Klemp, J. B., Skamarock, W. C., Davis, C. A., Dudhia, J., Gill, D. O., Coen, J. L., Gochis, D. J., Ahmadov, R., Peckham, S. E., Grell, G. A., Michalakes, J., Trahan, S., Benjamin, S. G., Alexander, C. R., Dimego, G. J., Wang, W., Schwartz, C. S., Romine, G. S., Liu, Z., Snyder, C., Chen, F., Barlage, M. J., Yu, W., and Duda, M. G.: The weather research and forecasting model: Overview, system efforts, and future directions, B. Am. Meteorol. Soc., 98, 1717–1737, https://doi.org/10.1175/BAMS-D-15-00308.1, 2017.

Risanto, C. B., Castro, C. L., Arellano, A. F., Moker, J. M., and Adams, D. K.: The impact of assimilating GPS precipitable water vapor in convective-permitting WRF-ARW on North American Monsoon precipitation forecasts over Northwest Mexico, Mon. Weather Rev., 149, 3013–3035, https://doi.org/10.1175/MWR-D-20-0394.1, 2021.

Rohm, W., Guzikowski, J., Wilgan, K., and Kryza, M.: 4DVAR assimilation of GNSS zenith path delays and precipitable water into a numerical weather prediction model WRF, Atmos. Meas. Tech., 12, 345–361, https://doi.org/10.5194/amt-12-345-2019, 2019.

Singh, R., Ojha, S. P., Puviarasan, N., and Singh, V.: Impact of GNSS signal delay assimilation on short range weather forecasts over the Indian region, J. Geophys. Res.-Atmos., 124, 9855–9873, https://doi.org/10.1029/2019JD030866, 2019.

Skamarock, W. C., Klemp, J. B., Dudhia, J., Gill, D. O., Barker, D. M., Duda, M. G., Huang, X., Wang, W., Powers, J. G.: A Description of the Advanced Research WRF Version 3, NCAR Tech. Note, https://doi.org/10.5065/D68S4MVH, 2008.

Thayer, G. D.: An improved equation for the radio refractive index of air, Radio Sci., 9, 803–807, https://doi.org/10.1029/RS009i010p00803, 1974.

Thompson, G., Field, P. R., Rasmussen, R. M., and Hall, W. D.: Explicit forecasts of winter precipitation using an improved bulk microphysics scheme. Part II: Implementation of a new snow parameterization, Mon. Weather Rev., 136, 5095–5115, https://doi.org/10.1175/2008MWR2387.1, 2008.

Thundathil, R., Zus, F., Dick, G., and Wickert, J.: Assimilation of GNSS tropospheric gradients into the Weather Research and Forecasting (WRF) model version 4.4.1, Geosci. Model Dev., 17, 3599–3616, https://doi.org/10.5194/gmd-17-3599-2024, 2024a.

Thundathil, R., Zus, F., Dick, G., and Wickert, J.: Assimilation of GNSS Zenith Delays and Tropospheric Gradients: A Sensitivity Study utilizing sparse and dense station networks, Zenodo [data set and code], https://doi.org/10.5281/zenodo.13734634, 2024b.

Václavovic, P., Douša, J., and Györi, G.: G-Nut software library – State of development and first results, Acta Geodyn. Geomater., 10, 431–436, https://doi.org/10.13168/AGG.2013.0042, 2014.

Vedel, H. and Huang, X. Y.: Impact of ground based GPS data on numerical weather prediction, J. Meteorol. Soc. Jpn. Ser. II, 82, 459–472, https://doi.org/10.2151/jmsj.2004.459, 2004.

Walpersdorf, A., Calais, E., Haase, J., Eymard, L., Desbois, M., and Vedel, H.: Atmospheric gradients estimated by GPS compared to a high resolution numerical weather prediction (NWP) model, Phys. Chem. Earth A, 26, 147–152, https://doi.org/10.1016/S1464-1895(01)00038-2, 2001.

Wang, Z., Bovik, A. C., Sheikh, H. R., and Simoncelli, E. P.: Image quality assessment: from error visibility to structural similarity, IEEE Trans. Image Process., 13, 600–612, https://doi.org/10.1109/TIP.2003.819861, 2004.

Wickert, J., Dick, G., Schmidt, T., Asgarimehr, M., Antonoglou, N., Arras, C., Brack, A., Ge, M., Kepkar, A., Männel, B., Nguyen, C., Oluwadare, T. S., Schuh, H., Semmling, M., Simeonov, T., Vey, S., Wilgan, K., and Zus, F.:GNSS Remote Sensing at GFZ: Ove: GNSS remote sensing at GFZ: Overview and recent results, ZfV-Z. Geod. Geoinf. Landmanag., 5/2020, https://doi.org/10.12902/zfv-0320-2020, 2020.

Yan, X., Ducrocq, V., Poli, P., Hakam, M., Jaubert, G., and Walpersdorf, A.: Impact of GPS zenith delay assimilation on convective-scale prediction of Mediterranean heavy rainfall, J. Geophys. Res.-Atmos., 114, https://doi.org/10.1029/2008JD011036, 2009.

Yang, S. C., Huang, Z. M., Huang, C. Y., Tsai, C. C., and Yeh, T. K.: A case study on the impact of ensemble data assimilation with GNSS-zenith total delay and radar data on heavy rainfall prediction, Mon. Weather Rev., 148, 1075–1098, https://doi.org/10.1175/MWR-D-18-0418.1, 2020.

Zus, F., Douša, J., Kačmařík, M., Václavovic, P., Dick, G., and Wickert, J.: Estimating the impact of GNSS horizontal delay gradients in variational data assimilation, Remote Sens., 11, 41, https://doi.org/10.3390/rs11010041, 2019.

Zus, F., Thundathil, R., Dick, G., and Wickert, J.: Fast Observation Operator for Global Navigation Satellite System TGs, Remote Sens., 15, 5114, https://doi.org/10.3390/rs15215114, 2023.

Zus, F., Balidakis, K., Dogan, A. H., Thundathil, R., Dick, G., and Wickert, J.: DNS (v1.0): An open source ray-tracing tool for space geodetic techniques, Geosci. Model Dev. Discuss. [preprint], https://doi.org/10.5194/gmd-2024-237, in review, 2025.